Structural Analysis of Bituminous Road Pavements Embedding Charging Units for Electric Vehicles

Claudia Nodari[1](✉), Maurizio Crispino[1], Mariano Pernetti[2], and Emanuele Toraldo[1]

[1] Department of Civil and Environmental Engineering, Politecnico di Milano, Piazza Leonardo da Vinci 32, 20133 Milan, Italy
claudia.nodari@polimi.it

[2] Department of Engineering, Università Della Campania "Luigi Vanvitelli", via Roma 29, 81031 Aversa, Caserta, Italy

Abstract. Among the arising technologies for electric mobility, the *on-the-road* (dynamic) vehicle charging appears to be a promising solution in order to overcome the current limitations of the electric vehicles' batteries. For achieving this purpose, the use of Charging Units (CUs) embedded into the road pavements is needed. These CU are made of a cement concrete box in which the electric technologies are allocated. However, the CUs have not to be detrimental for the structural behavior of the pavements, including their load resistance performances.

The lack of scientific studies in the available literature demonstrate that the topic is not fully investigated. Moreover, the available scientific papers assume the CU as a solid, not considering it as a box (having a void for the electric technologies). However, it is a key factor for the pavements' structural response.

This is the reason why this research was devoted to assess the structural response of electrified roads (*e-road*s), in which the CUs are embedded, compared to the traditional roads (*t-road*s), using a Finite Element Modelling (FEM) approach. Therefore, the main scope of this study is the optimization of the void dimensions into CU from a pavement structural performances point of view. The optimization included different cross-sectional geometries and load positions. As a result of these FEM investigations, a first set of interesting outcomes were obtained, as shown and discussed in the paper.

Keywords: Electrified road · Dynamic charging · Charging Unit (CU) · Finite Element Modelling (FEM) · Structural analysis · Bituminous pavements

1 Introduction

As the European Commission report 2019 shown, in the EU-28 transport generates 32.1% of the total Green House Gases (GHG) emissions and road transport is responsible for 71.7% of the sector's emissions [1]. In this framework and in line with EU policy to climate neutrality by 2050 [2], the electrification of vehicles is a possible solution to enhancing road sector environmental sustainability [3–5].

© Springer Nature Switzerland AG 2021
O. Gervasi et al. (Eds.): ICCSA 2021, LNCS 12952, pp. 149–162, 2021.
https://doi.org/10.1007/978-3-030-86973-1_11

In this view, several environmental benefits can be obtained by the use of Electric Vehicles, this is the reason why this technology is becoming very much attractive [4, 6]. In particular, Battery Electric Vehicles (BEV) are entirely powered by batteries, without any internal combustion engine (ICE) [7]. However, some handicaps restrain their potential application [4, 5, 8]: high initial cost, long waiting time and short range, better known as *range anxiety* (i.e. an EV driver's fear of running out of electricity before reaching another available charging station [9]). Therefore, on-the-road (dynamic) charging appears to be a promising solution to overcome the current limitations [4, 8, 10], but it requires a proper charging infrastructure network [11]. Thus, traditional road (*t-road*) becomes electrified road (*e-road*) if it is able to deliver the electrical power to charge the EV efficiently using specific conductive or contactless charging systems, as stated in [4].

2 Literature Review

According to the available literature, two charging methods are nowadays considering a promising option: conductive and contactless technologies [4, 5]. In the first case, a practical connection mode is used to link vehicle to the charging infrastructure. Some examples are overhead pantograph or conductive track mounted on the road surface, as shown in Fig. 1a and Fig. 1b, respectively. As regards contactless charging, Wireless Power Transmission (WPT) system is adopted to deliver electrical energy to the electric vehicle at a gap distance. Being a near-field WPT charging technology, the Inductive Power Transfer (IPT) charging has shown good performance [4].

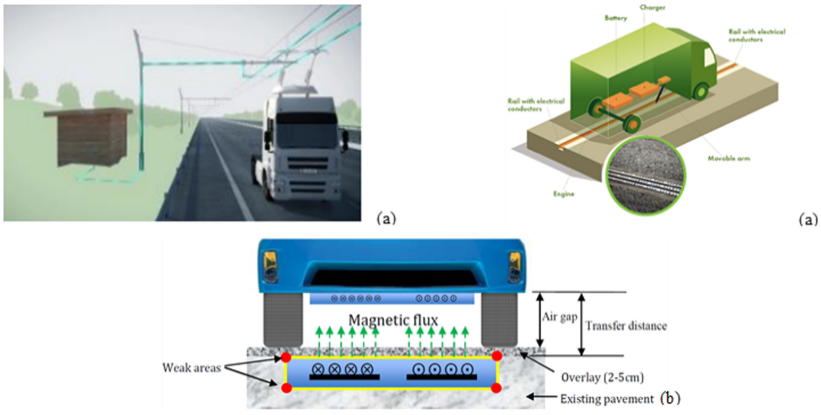

Fig. 1. Examples of charging systems (a) conductive [12, 13] (b) contactless [4]

Considering dynamic inductive charging technology, the use of prefabricated Charging Unit (CU) embedded into flexible pavement is a possible solution, as suggested by the available scientific literature [5, 14]. As presented in [5], it is possible to classify construction technologies of embedded charging systems into two categories: prefabrication-based construction method and on-site construction method. In the first case, CU are

built in the factory as prefabricated modulus and then embedded on-site in short period. In the second one, all the facilities are prepared and installed on-site.

CU normally is composed of power electronic device protected by a concrete slab from traffic-induced damages [15] and water aggression [4, 15]: CU is a concrete box in which the electric technologies are allocated.

Currently, contactless charging has shown good performance as a battery charging technology [4]. However, there are few studies in literature on the structural behavior of this type of composite pavement. In other words, the available scientific literature is not able to demonstrate the effects of the CU on the pavement structural response and how it affects the pavement lifetime. Thus, the research described in this paper focuses on the aforementioned topics, particularly focusing on the structural response of *e-road*, evaluating the effects of CU in comparison with a standard *t-road* solution. It was performed by developing a Finite Element Model (FEM). Therefore, the novelty is not the model, since it is well known at the state of the art of pavement structural calculations, but the road pavement itself, in which CUs are embedded for electric vehicles charging. Moreover, the aforementioned scientific papers assume the CU as a solid, not considering it as a box (having a void for allocating the electric technologies). Therefore, to be a step ahead of the current *e-road* state of art, the FEM calculations consider the prefabricated concrete CU both as a solid box (solid CU) and as a hollow box (void CU). Consequently, the present study has two stages. In the first phase, structural behaviors of *t-road* and *e-road* with solid box (*e-road_solid CU*) are compared to evaluate solid CU effect. In the second step, a void CU is studied in order to optimize the dimension of the void from a pavement structural response point of view. Thus, to gain the optimum void CU geometry, several simulations are performed progressively increasing hollow dimension. Finally, a comparison between *e-road_solid CU* and different *e-road_void CU* geometries is made, considering the effects of the voids into the CU on the pavement stress-strain.

The paper is planned as follows. The adopted methodology is detailed in Sect. 3. Section 4 shows the effect of solid CU into the road pavement, in terms of stresses, for different load positions. Section 5 analyses the effect of void CU, considering various void dimensions and load positions. In Sect. 6 the procedure for void CU optimization is described. Finally, conclusions and future studies are drawn in Sect. 7.

3 Methodology

As mentioned above, the research is divided in two stages, in which different cross-sectional geometries are studied (Sect. 3.1). Moreover, three different load positions are evaluated for considering the absence of drivers' physical constraints in choosing their road paths. In fact, vehicles can move along road cross direction with a certain wander distance. Considering these conditions, 15 simulations are carried out using a FEM software to calculate stresses and strains throughout the domain.

A 2D model is built for simulating the structural behavior of pavements (*t-road* and *e-road)* subjected to traffic. For the sake of simplicity, an elastic model is assumed to be acceptable for all materials, even if more precise models have been developed as viscoelastic-viscoplastic one with damage coupled for asphalt materials [16]. Each layer is defined as isotropic-linear-elastic material, so marked by thickness, Young's

modulus, and Poisson's Ratio. Such a model has been implemented by using COMSOL Multiphysics 5.5. The equations used are shown below: equilibrium Eq. (1), constitutive equation based on Hooke's law (2) and strain-displacement (6) equations.

$$div\sigma + F_v = 0 \tag{1}$$

$$\sigma = \sigma_{ex} + \mathbb{D} \cdot \varepsilon_{el} \tag{2}$$

$$\varepsilon_{el} = \varepsilon - \varepsilon_{inel} \tag{3}$$

$$\varepsilon_{inel} = \varepsilon_0 + \varepsilon_{ext} + \varepsilon_{th} + \varepsilon_{hs} + \varepsilon_{pl} + \varepsilon_{cr} + \varepsilon_{vp} \tag{4}$$

$$\sigma_{ex} = \sigma_0 + \sigma_{ext} + \sigma_q \tag{5}$$

$$\varepsilon = 1/2 \cdot \left(\nabla u + \nabla u^T\right) \tag{6}$$

$$\mathbb{D} = \mathbb{D}(E, \nu) \tag{7}$$

Where:
σ = stress tensor;
F_v = Volume force vector;
$\mathbb{D}$ = 4th order elasticity tensor;
ε = strain tensor;
ε_{el} = elastic strain tensor;
ε_{inel} = inelastic strain tensor; inelastic strain tensor contributions: ε_0 = initial strain; ε_{ext} = external strain; ε_{th} = thermal strain; ε_{hs} = hygroscopic strain; ε_{pl} = plastic strain; ε_{cr} = creep strain; ε_{vp} = viscoplastic strain;
σ_{ex} = extra stress tensor; extra stress tensor contributions: σ_0 = initial stress; σ_{ext} = external stress; σ_q = extra stress caused by viscous damping;
∇u = displacement gradient tensor;
E = Young's modulus;
ν = Poisson's Ratio.

3.1 Geometry and Materials

As already stated, various cross-sectional geometries were analyzed for *t-road* and *e-road*. Figure 2 shows the geometries considered in this study. Figure 2a describes a *t-road* as a semi-rigid pavement. Thickness of wearing course is selected in the typical reference range of 40-50 mm [17] to reduce the energy transfer distance, with better results in battery charging [4]. Based on this sketch, prefabricated CU is embedded in the middle of the lane within a single asphalt layer, obtaining a composite pavement cross section. CU is assumed to have a size of 0.14 m in height and 0.8 m in width, as introduced in Chen's study [4]. In Fig. 2b, CU is considered as a solid box, as the current state of art [4, 5]. Figure 2c, Fig. 2d and Fig. 2e, instead, suggest new *e-road*

cross-sectional geometries in which the prefabricated CU has an opening in the middle with different void dimensions (more details are given in Sect. 6).

The characteristics of each layer and/or material are reported in Table 1, based on typical material properties. As regard asphalt, Young's modulus refers to mean value of stiffness modulus evaluated at a temperature of 20 °C and load frequency equal to 2 Hz. As mentioned before the CU is made of cement concrete and an isotropic behavior [15] is assumed.

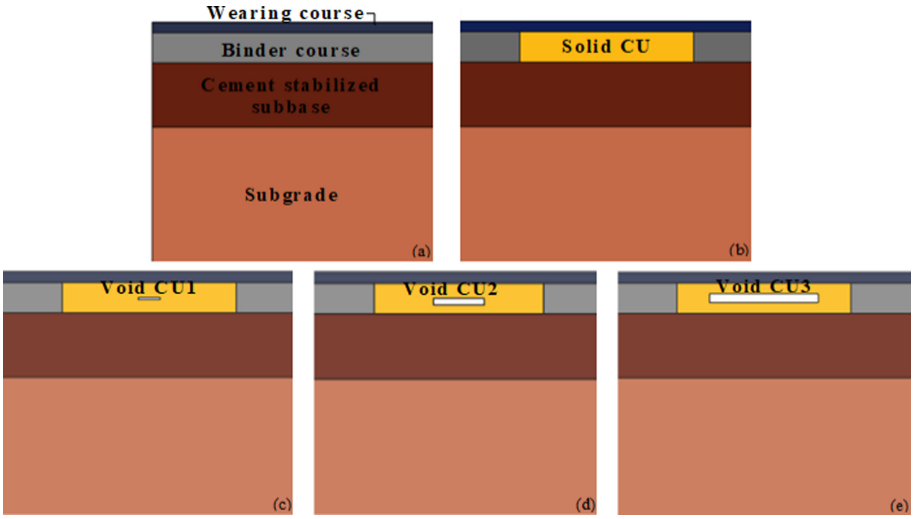

Fig. 2. Cross-sectional geometry (a) *t-road* (b) *e-road_solid CU* (c-e) *e-road_void CU*

Table 1. Key material main characteristics

	Thickness [m]	Bulk density [N/m^3]	Young's modulus [N/mm^2]	Poisson's ratio [-]
Wearing course	0.05	24,000	5,500	0.35
Binder course	0.14	23,500	3,500	0.35
Cement stabilized subbase	0.30	23,000	2,000	0.20
Subgrade	6.00	21,000	800	0.30
Concrete CU	0.14	23,000	25,000	0.20

3.2 Loads and Boundary Conditions

Model boundary conditions are shown in Fig. 3. The 2D model is assumed to be symmetric, along the road symmetry axis. A roller constraint is used at the bottom of the

thick subgrade and on the right of the model, to put equal to zero the displacement in the direction perpendicular (normal) to the boundary. The default boundary condition is free on the surface, except for the area in which the load acts. As shown in Fig. 3(b), a total number of 7,456 triangular elements are built and finer elements are established around CU corners. Three different load positions are considered to explain cross wander distance compared to CU location, as reported in Fig. 4. In the first one, the load is centered on CU (Fig. 4a). The lateral displacements are also considered: left wheel is on the CU left edge (Fig. 4b), left wheel is located at the CU center (Fig. 4c). Concerning load characteristics, a single static tire with a contact pressure of 0.8 N/mm^2 (800 kPa) and a tire width of 0.2 m are used to simulate a road heavy vehicle loading; a wheel axis of 1.56 m length is assumed [5].

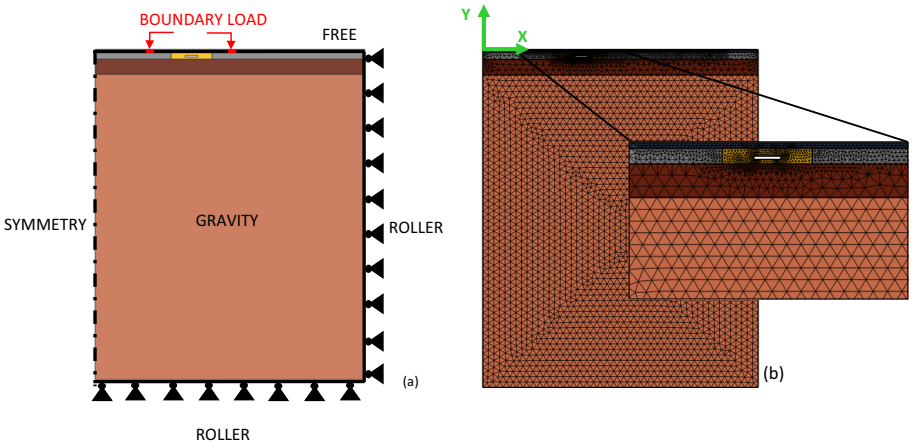

Fig. 3. (a) Loads and boundary conditions (b) FE mesh

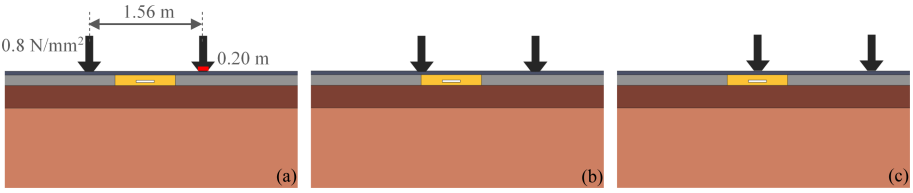

Fig. 4. Load positions (a) centered on CU (b) CU edge (c) CU center

4 Effects of Solid CU into the Road Pavements

Among the several outputs of the FEM calculations, the stresses are considered in this study. In Fig. 5 and in Fig. 6 the stress FEM results are shown for both *t-road* and *e-road_solid CU*, according to the three load positions previously described.

Focusing on Fig. 5, the FEM results reveal that the vertical stress σ_{yy} is close to the applied load, which penetrates and vanish gradually downward, according to the results obtained in the Chen's study [5]. As regard *e-road_solid CU*, when load is centered on CU or on CU center, a similar stress distribution can be seen. When load is located on the CU edge, instead, stress distribution changes near CU left edge. At the left margin out of CU, stress in compression decreases of 60% compared to *t-road*; in the middle of CU, compression stress increases by more than 55% respect to *t-road*. In the last load position, along CU center, it is possible to observe a decrease of stress in compression of 66% compared to *t-road*. Moreover, stress increases in the area outside CU lateral edge by 130% compared to the traditional pavement.

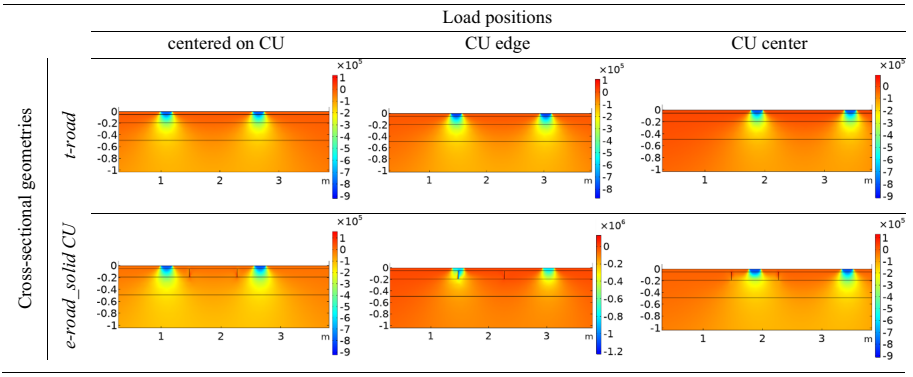

Fig. 5. Distribution of vertical stress σ_{yy} at different cross-sectional geometries and different load positions

As regard horizontal stress (Fig. 6), it can be observed that stress field mostly changes according to cross-sectional geometry and load position. The FEM outputs show that

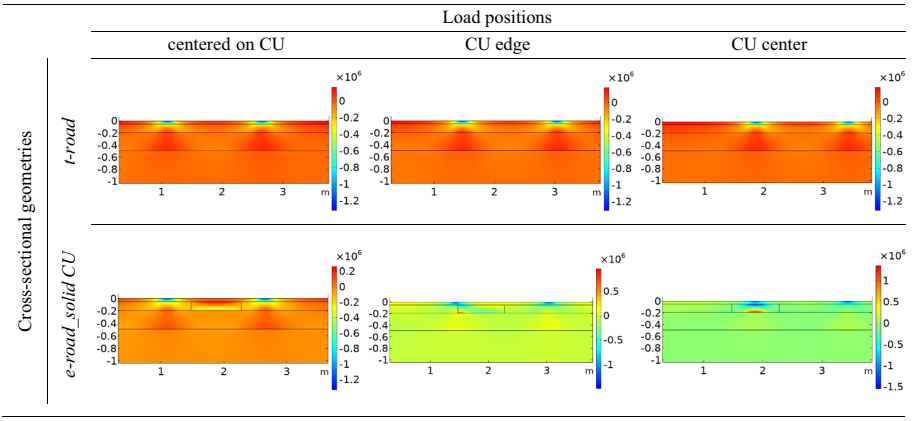

Fig. 6. Distribution of horizontal stress σ_{xx} at different cross-sectional geometries and different load positions

significant horizontal stresses σ_{xx} in compression appears on the pavement surface close to the area of load application, confirming the results reported in [5].

Moreover, tensile stresses are concentrated at the bottom of cement stabilized subbase layer of the *t-road*. Considering the *e-road*, when load is centered on CU, compressive stresses arise at the bottom of CU (an increase of four time is observed in comparison with the *t-road* results). If the load is on CU edge, *e-road* results show tensile stresses at the CU left edge bottom corner. In detail, considering left edge out, stress increases by 230% compared to the *t-road*. In the last load position (CU center) stress concentration rises in CU: at the CU top it is possible to note an increase of compression stress (270% compared to the *t-road* outputs), at CU bottom, the tensile stress can be evaluated 13 times higher than the *t-road* results.

5 Effects of Void CU into the Road Pavements

In Fig. 7 and Fig. 8, FEM results in terms of stress are shown for both *e-road_solid CU* and *e-road_void CU* at different load positions. Focusing on Fig. 7, when the load axle is centered on CU and when the wheel is on CU edge, it can be noted that σ_{yy} is below the applied load which penetrates and vanish gradually downward. Such a behavior is similar to the one described in the previous section. On the contrary, when the load is on the

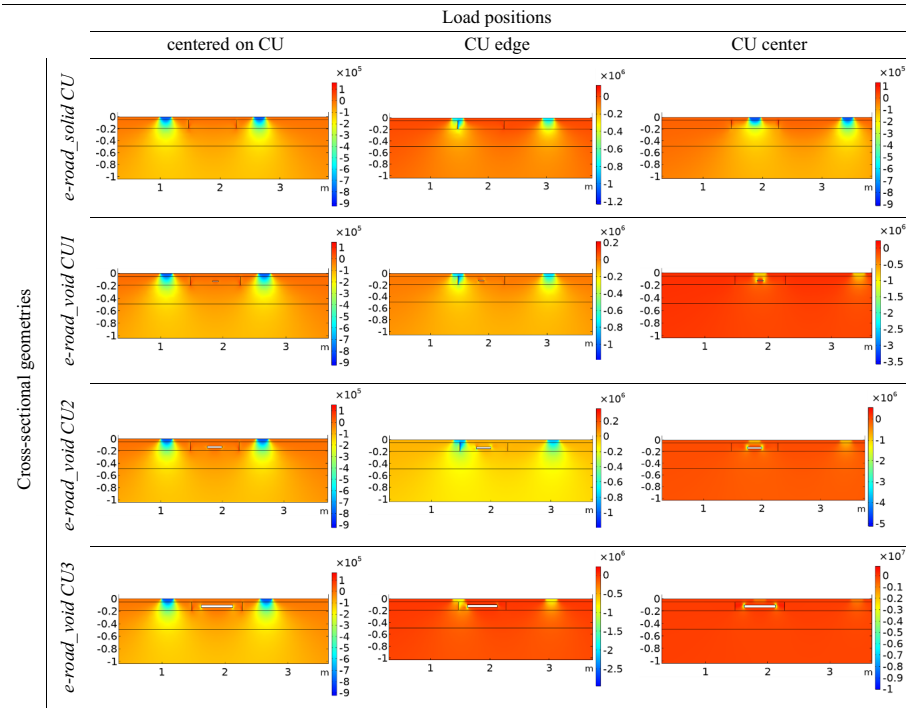

Fig. 7. Distribution of vertical stress σ_{yy} at different cross-sectional geometries of *e-road* and different load positions

CU center, stress distribution changes compared to *e-road_solid CU*. It is still possible to observe light stress under load, but there is a compressive stress concentration around CU void, that increases with void dimension. In particular, stress in compression at the top left corner of cavity increases by 72% (*e-road_void CU2*) and by 234% (*e-road_void CU3*) compared to *e-road_void CU1*.

As regard horizontal stress (Fig. 8), it can be observed that stress field mostly changes according to load position. All the FEM simulations reveal that significant σ_{xx} in compression appears on the pavement surface close to the applied load, as presented in the previous section. When load is centered on CU, some compressive stresses arise at the bottom of CU itself. Moreover, tensile stresses concentrate at the bottom of cement stabilized subbase layer.

If the load is on CU edge, tensile stresses grow at left bottom corner of the CU, an increase of 10% for both *e-road_void CU1* and *e-road_void CU2* in comparation with the solid CU results; in the case of *e-road_void CU3* it increases up to 36%. Further, at left top corner of the cavity, it is possible to note the arising of tensile stresses according to the cavity dimension increase. It can be estimated at a magnitude of 330% for *e-road_void CU2* and more than 740% for *e-road_void CU3*, once again in comparation to *e-road_void CU1* results. At left bottom corners of cavity, the compression stresses also arise (an increase of 208% and 572% is found, respectively).

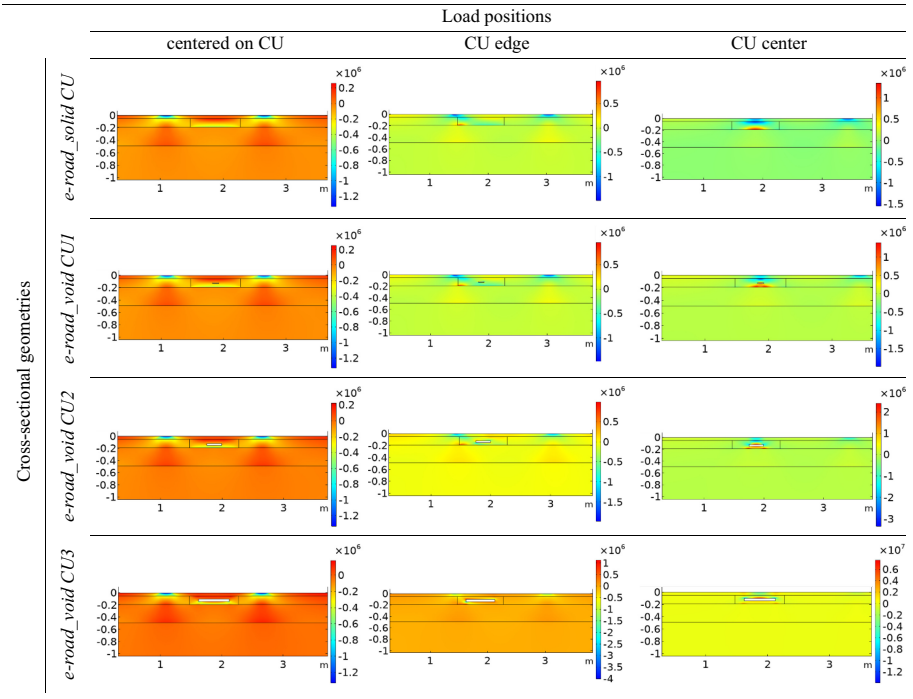

Fig. 8. Distribution of horizontal stress σ_{xx} at different cross-sectional geometries of *e-road* and different load positions

In the last load position (CU center), a stress concentration rising on the CU is appreciable. In detail, at the CU top the compression stress arise according to the cavity dimension, passing from 27% for the *e-road_void CU3*, to the 85% for the *e-road_void CU2* and exceeding the 240% for the *e-road_void CU1*. Moreover, tensile stresses can be observed at the bottom of the CU, such stresses increase according to the cavity dimension: by 13%, 35% and 128% compared to solid CU outputs, respectively.

In addition, it can be observed that some tensile stresses rise on the top and on the bottom of CU cavity. In the first case, an increase of more than 725% (*e-road*_void CU3) and 160% (*e-road_void CU2*) compared to *e-road_void CU1* is recorded. In the second case, stresses gain 113% and 157%, respectively, compared to *e-road_void CU1*.

6 Optimization of *Void CU* Dimension

As already stated, in order to achieve the optimum void CU geometry, several FEM simulations are performed progressively increasing void dimension. A comparison between different *e-road_void CU* geometries is made, as described in Sect. 5. The cavity dimension into the CU is optimized comparing the FEM stress outputs with the failure tensile/compression stresses of the materials of both layers and charging unit (Table 2).

For the CU cavity optimization purposes, even if the FEM stress outputs are calculated throughout the entire pavement domain using FE model, the structural comparison is performed along defined sections of analysis, as reported in Fig. 9. *Left section* and *Right section* match to load positions when load is centered on CU (Fig. 4a). *CU_left edge out* is 5 mm off CU left edge. Moreover, *CU_left edge in* is 5 mm within CU left edge. Similarly, for the right end. *CU center, CU_left edge center* and *CU_right edge center* sections are in the middle of CU, CU left edge and CU right edge, respectively.

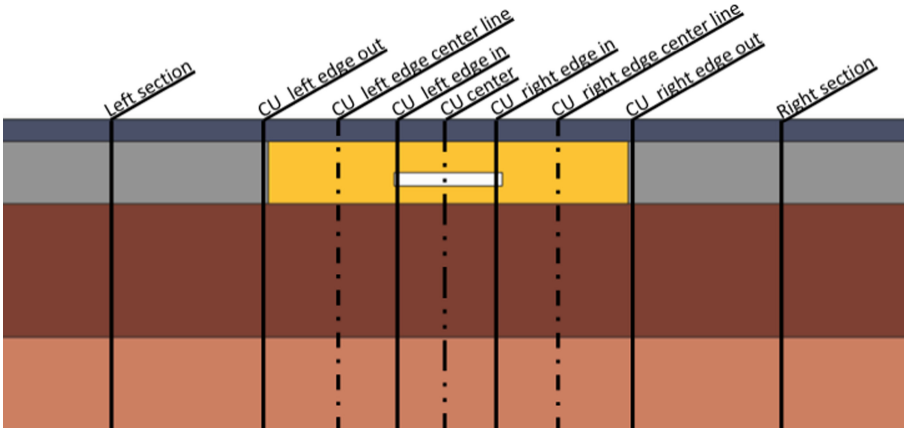

Fig. 9. Vertical analysis sections (y-direction)

The horizontal analysis is performed on the layers' interfaces, as shown in Fig. 10. Two sections are evaluated per each interface, at +1 mm (top) and −1 mm (down) from the interface. The surface of wearing course is also analyzed.

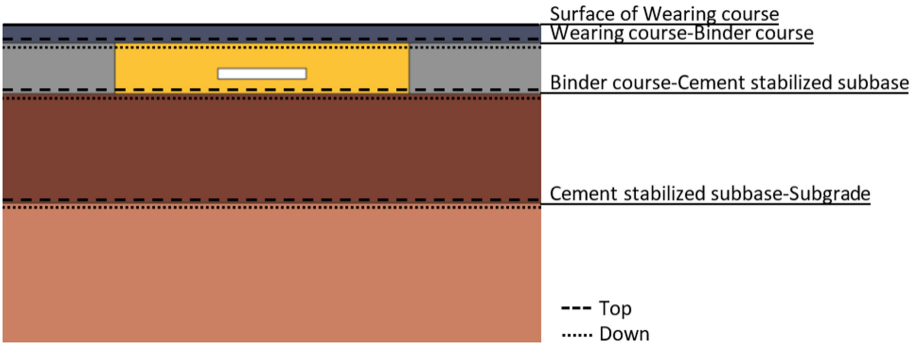

Fig. 10. Horizontal analysis sections (x-direction)

Therefore, the FEM stress outputs along these sections are compared with the failure tensile/compression stresses of the materials composing each layer. Acceptable results are achieved for *e-road_void CU1* and *e-road_void CU2*, instead *e-road_void CU3* failed, as suggested by the results discussed in the previous Sect. 5.

The final choice falls on *e-road_void CU2*, since it is the solution that maximize the cavity dimension maintaining the stress levels of the whole pavement lower than the failure stresses of the component materials. In Fig. 11 the details of the selected void CU are given.

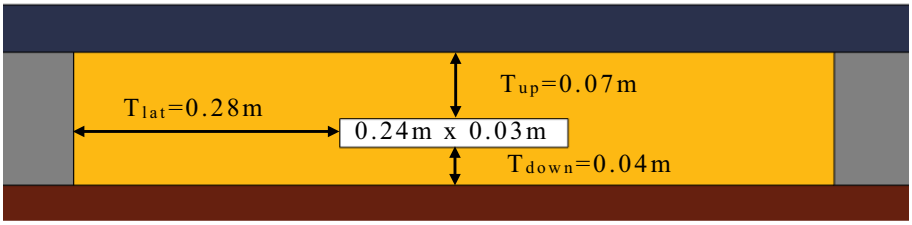

Fig. 11. Void CU details

Table 2 shows the comparison between the maximum FEM stress outputs, calculated in the optimized void CU, and failure tensile/compression stresses of the materials of both layers and charging unit.

Table 2. Comparison between maximum FEM stresses in optimized void CU and failure tensile/compression stresses

			Materials			
			Wearing course	Binder course	Cement stabilized subbase	Concrete
$\sigma_{xx,tens}$	Max FEM stress	Value [N/mm^2]	0.18	0.31	0.15	2.20
		Load position	CU center	CU edge	CU edge	CU center
		Analysis section	Surface of wearing course	Binder course - cem.stab subb._ Top	Binder course - cem.stab subb._ Down	Binder course - cem.stab subb._ Top
	Failure tensile stress [N/mm^2]		1.25[a]	1.55[b]	0.50[c]	2.21
$\sigma_{xx,comp}$	Max FEM stress	Value [N/mm^2]	−1.58	−0.56	−0.14	−3.15
		Load position	CU center	CU edge	CU center	CU center
		Analysis section	CU center	Wearing course - binder course_ Down	Binder course - cem.stab subb._ Down	CU_left edge in
	Failure tensile stress [N/mm^2]		−3.75	−4.65	−1.50	−20.00
$\sigma_{yy,comp}$	Max FEM stress	Value [N/mm^2]	−1.13	−0.76	−0.46	−1.30
		Load position	Centered on CU	CU edge	CU edge	CU center
		Analysis section	Surface of wearing course	Wearing course - binder course_ Down	Binder course - cem.stab subb._ Down	CU_right edge in
	Failure tensile stress [N/mm^2]		−6.25	−7.75	−4.00	−20.00[d]

[a]Value in the interval 1.11–1.67 MPa [18]
[b]Value in the interval 1.20–1.55 MPa [19]
[c]Value in the interval 0.43–0.55 MPa [20]
[d]Considering C20/25 [21]

7 Conclusions

The electrification of vehicles is a possible solution to enhancing road sector environmental sustainability. On-the-road charging appears to be a promising solution to overcome the current limitations of batteries, but it requires a proper charging infrastructure network. For this purpose, traditional road needs to be converted in electrified road. This research focuses on structural response of electrified road pavement compared to the traditional one, using a Finite Element Modelling approach, considering both the charging unit a solid box, as suggested by the available scientific literature, and a void box for allocating the electronic devices.

As a summary of the obtained results, the following conclusions can be drawn.

Considering the Charging Unit as a Solid Box, the results previously described suggest that small differences exist between *t-road* and *e-road*, considering the stresses to which the pavement is subjected on the vertical direction. On the contrary, considering the horizontal direction, an increase of stresses on the pavement close to the CU can be expected; thus, the CU changes the pavement stress distribution.

The results about the Void Charging Unit reveal that it has a non-negligible impact on the structural response, making the pavement more vulnerable to load position effects. Furthermore, the stresses to which both the CU and the pavement are subjected increase according to the cavity dimension. However, these stresses can be managed, optimizing the CU cavity dimension, in order to maintain them lower than the failure tensile/compression stresses of the materials composing the pavement layers (including the CU).

Obviously, the results reported in the paper can be considered as a first step in the comprehension of the CU structural effects on road pavements. Some issues remain still open (e.g. the effects of temperature changing, fatigue and rutting on the bituminous layers behavior, surface distresses) and must be optimized (e.g. the charging unit shape considering a fillet-shaped exterior corner) in further studies.

References

1. Commission, E.: EU Transport in figures - Statistical Pocketbook 2019 (2018). https://doi.org/10.2832/017172
2. Commission, E.: The European Green Deal (2019)
3. Nicolaides, D., Cebon, D., Miles, J.: An urban charging infrastructure for electric road freight operations: a case study for Cambridge UK. IEEE Syst. J. **13**, 2057–2068 (2019). https://doi.org/10.1109/JSYST.2018.2864693
4. Chen, F., Kringos, N.: Towards new infrastructure materials for on-the-road charging. In: 2014 IEEE Int. Electr. Veh. Conf. IEVC 2014, pp. 1–5 (2015). https://doi.org/10.1109/IEVC.2014.7056235
5. Chen, F., Balieu, R., Córdoba, E., Kringos, N.: Towards an understanding of the structural performance of future electrified roads: a finite element simulation study. Int. J. Pavement Eng. **20**, 204–215 (2019). https://doi.org/10.1080/10298436.2017.1279487
6. Karmaker, A.K., Roy, S., Ahmed, M.R.: Analysis of the impact of electric vehicle charging station on power quality issues. In: 2nd Int. Conf. Electr. Comput. Commun. Eng. ECCE 2019, pp. 7–9 (2019). https://doi.org/10.1109/ECACE.2019.8679164

7. Ajanovic, A.: The future of electric vehicles: prospects and impediments. Wiley Interdiscip. Rev. Energy Environ. **4**, 521–536 (2015). https://doi.org/10.1002/wene.160
8. Gill, J.S., Bhavsar, P., Chowdhury, M., Johnson, J., Taiber, J., Fries, R.: Infrastructure cost issues related to inductively coupled power transfer for electric vehicles. Procedia Comput. Sci. **32**, 545–552 (2014). https://doi.org/10.1016/j.procs.2014.05.459
9. Pevec, D., Babic, J., Carvalho, A., Ghiassi-Farrokhfal, Y., Ketter, W., Podobnik, V.: A survey-based assessment of how existing and potential electric vehicle owners perceive range anxiety. J. Clean. Prod. **276** (2020). https://doi.org/10.1016/j.jclepro.2020.122779
10. Venugopal, P., et al.: Roadway to self-healing highways with integrated wireless electric vehicle charging and sustainable energy harvesting technologies. Appl. Energy. **212**, 1226–1239 (2018). https://doi.org/10.1016/j.apenergy.2017.12.108
11. Throngnumchai, K., Hanamura, A., Naruse, Y., Takeda, K.: Design and evaluation of a wireless power transfer system with road embedded transmitter coils for dynamic charging of electric vehicles. In: 2013 World Electr. Veh. Symp. Exhib. EVS 2014, pp. 1–10 (2014). https://doi.org/10.1109/EVS.2013.6914937
12. Chairman, F.B.– B.S. p. A.: eHighway - per il trasporto elettrico delle merci. http://www.brebemi.it/site/wp-content/uploads/2019/03/A35Brebemi_EMotorway_Francoforte.pdf. Accessed 23 Nov 2020
13. eRoadArlanda. https://eroadarlanda.com/the-technology/. Accessed 23 Nov 2020
14. Chabot, A., Deep, P.: 2D Multilayer solution for an electrified road with a built-in charging box. Road Mater. Pavement Des. **20**, S590–S603 (2019). https://doi.org/10.1080/14680629.2019.1621445
15. Chen, F., Coronado, C.F., Balieu, R., Kringos, N.: Structural performance of electrified roads: a computational analysis. J. Clean. Prod. **195**, 1338–1349 (2018). https://doi.org/10.1016/j.jclepro.2018.05.273
16. Chen, F., Balieu, R., Kringos, N.: Thermodynamics-based finite strain viscoelastic-viscoplastic model coupled with damage for asphalt material. Int. J. Solids Struct. **129**, 61–73 (2017). https://doi.org/10.1016/j.ijsolstr.2017.09.014
17. Ceravolo, R., Miraglia, G., Surace, C., Zanotti Fragonara, L.: A computational methodology for assessing the time-dependent structural performance of electric road infrastructures. Comput. Civ. Infrastruct. Eng. **31**, 701–716 (2016). https://doi.org/10.1111/mice.12199
18. Zemedkun, B.S., Takahashi, O.: Demarcation study on reclaimed asphalt pavement contents in recycled hot mix asphalt mixtures for wearing course in asphalt pavements. Int. J. Adv. Sci. Eng. Inf. Technol. **10**, 1571–1577 (2020). https://doi.org/10.18517/ijaseit.10.4.3946
19. Topini, D., Toraldo, E., Andena, L., Mariani, E.: Use of recycled fillers in bituminous mixtures for road pavements. Constr. Build. Mater. **159**, 189–197 (2018). https://doi.org/10.1016/j.conbuildmat.2017.10.105
20. Toraldo, E., Mariani, E., Crispino, M.: Laboratory investigation into the effects of fibres and bituminous emulsion on cement-treated recycled materials for road pavements. Eur. J. Environ. Civ. Eng. **20**, 725–736 (2016). https://doi.org/10.1080/19648189.2015.1061460
21. European Commission: Concrete - Part 1: Specification, performance, production and conformity. EN 206–1